Design, manufacturing and prototype testing of the METIS ring apodizer

Lorenzo König[a,b], Christian Delacroix[a], Olivier Absil[a], and Gilles Orban de Xivry[a]

[a]STAR Institute, Université de Liège, Allée du Six Août 19C, 4000 Liège, Belgium
[b]Jet Propulsion Laboratory, California Institute of Technology, 4800 Oak Grove Dr, Pasadena 91109 CA, USA

ABSTRACT

The Mid-Infrared ELT Imager and Spectrograph (METIS) is one of the three first-generation instruments of the Extremely Large Telescope (ELT). METIS will enable high-contrast imaging through different coronagraphic modes, one of which is implemented with a vortex coronagraph. However, the complex pupil of the ELT with its large central obscuration limits the performance of a classical vortex coronagraph. Using a grayscale ring apodizer in a pupil plane upstream of the vortex phase mask can correct for the effect of the central obscuration and partly restore the coronagraphic performance of the vortex for the ELT pupil. The coronagraphic performance of the ring-apodized vortex coronagraph relies on the precise control of transmission in the grayscale region, which can be implemented using a technology based on chromium microdots. Here, we present the ring apodizer for the METIS instrument exploiting the microdots technology. We first describe the design process of microdot patterns and perform simulations for both transmission and phase response of the microdots with various geometric parameters. We then describe the manufacturing of three prototypes featuring different design parameters, as well as their testing in terms of transmission and phase response. Finally, capitalizing on the lessons learned, we report on the current status of manufacturing and testing of the final ring apodizer for METIS.

Keywords: ring apodizer, vortex coronagraph, microdots, extremely large telescope

1. INTRODUCTION

The Extremely Large Telescope (ELT)[1] will enable revolutionary science in many areas of astronomy. One of its three first light instruments will be the Mid-Infrared ELT Imager and Spectrograph (METIS).[2] METIS will cover a broad range of science cases, including high-contrast imaging of exoplanets. Its spectral range covers the astronomical L, M and N-band atmospheric windows from 2.9 to 13.1 µm. With its imaging and spectroscopy modes in particular, METIS will advance the study and understanding of exoplanets and their atmospheres.

The METIS instrument features a series of high-contrast imaging and spectroscopy modes specifically designed for the detection and characterization of exoplanets.[3] One of the most promising modes for exoplanet characterization with METIS is the vortex coronagraph. METIS features a vortex coronagraph mode for each of its three bands: L ($2.9 - 4.1\,\mu m$), M ($3.9 - 5.1\,\mu m$) and N ($8.1 - 13.1\,\mu m$).[4] In theory, a vortex coronagraph provides perfect starlight rejection for a circular unobstructed pupil. However, the vortex coronagraph performs significantly worse in the presence of large central obscurations, as is the case for the ELT pupil. Moreover, the segmented primary mirror and the support structure holding the secondary mirror degrade the performance of the vortex coronagraph further.

The performance of the vortex coronagraph in presence of a circular central obscuration can be restored by introducing an apodizing mask in an upstream pupil plane.[5] In the case of a charge-2 vortex (as used in METIS) the pupil plane apodizer consists of a grayscale mask featuring a single grayscale ring of a certain radius and transmission. The optimal size and transmission of the grayscale ring are defined by the size of the central obscuration. METIS provides the ring-apodized vortex coronagraph mode (RAVC) in L and M-band. The RAVC is not provided for the N-band because it implies a lower overall throughput which is critical in the N-band due to the higher sky background emission.

In this manuscript we present the design, manufacturing and prototype testing of the METIS ring apodizer. Section 2 describes the design simulations characterizing the microdot patterns. In Section 3 we present three

intermediate prototypes validating our simulation framework in an experimental setup. Section 4 describes the design and fabrication of the METIS ring apodizer. Section 5 concludes this study and outlines the final characterization steps of the ring apodizer.

2. DESIGN AND SIMULATION OF THE MICRODOT PATTERNS

The property of the ring-apodized vortex coronagraph (RAVC) to restore the perfect starlight cancellation of the vortex relies on the careful control of transmission in the grayscale ring. It is therefore crucial to control this parameter across the desired wavelength range. One suited technology to create a grayscale apodizer is based on a microdot technology. This technology uses reflective chromium microdots with a size of a few times the wavelength[6] to create an effective grayscale transmission. The microdot technology is well-mastered[7] and apodizers based on microdot patterns have been used previously in the context of high contrast imaging.[8,9] The microdots technology has the advantage of being achromatic in phase and transmission making it ideally suited for the fabrication of the ring apodizer. Additionally, the phase introduced by the microdots is minimal, which is important for the working principle of the RAVC based on a pure amplitude mask. Other potential technologies to create a ring apodizer exist, such as transmissive grayscale components relying on thin layers of metals and dielectrics, and have been successfully applied to coronagraphy.[10] For METIS, the microdot technology based on chromium microdots printed on a coated ZnSe substrate has been chosen to fabricate the ring apodizer.

Here, the optimal conception of the microdot pattern is discussed. The goal of the microdot pattern is to provide the desired transmission across the pupil while limiting phase distortions due to the microdot technology. Rigorous coupled-wave analysis (RCWA)[11] is used to study the response of the microdot pattern to an incident beam, and find an optimal solution providing the desired transmission and maintaining a flat wavefront at the same time.

The algorithm to create the microdot pattern is based on an error-diffusion code.[12] This method is used to visualize grayscale patterns using binary pixel values, as done in inkjet printers or binary displays.[13] Error diffusion takes a grayscale array as input and sweeps across all pixels deciding whether a pixel is closer to be considered opaque or transparent. The difference between the desired grayscale value of a pixel and its imposed binary value is then diffused to the adjacent pixels which have not yet been processed. The error is diffused according to a scheme defined by the kernel of the error diffusion algorithm, which determines how the error is spread across the adjacent pixels. In this way, the desired grayscale is achieved on a macroscopic scale while the pattern consists of binary pixels on a microscopic scale. Here, the microdots are implemented by depositing a thin chromium layer on a substrate in each opaque pixel, while no chromium is present in the transparent pixels.

For filling factors that are close to a ratio of small integers, the microdot pattern becomes periodic. This can create diffraction artifacts affecting the amplitude and phase response of the pattern and therefore the resulting effective transmission. The effective transmission of periodic patterns depends on the exact microdot pattern, and not only the filling factor, unlike for random patterns. This is because a specific filling factor can be obtained using different periodic patterns, each one with a specific phase and amplitude response, while for random patterns there is no discrete diffraction orders but rather a lot of faint orders creating a sort of halo around the 0th order. It is therefore necessary to avoid integer fractions for the filling factor and add a small offset if necessary. In the case of chromium microdots, integer fractions can be avoided for the filling factor by tuning the remaining parameters of the pattern, which are the dot size and the chromium layer thickness. Another issue to consider is the behavior of the error-diffusion algorithm close to sharp borders aligned with the pixel axes (horizontal or vertical), which tend to be more periodic than parts of the pattern that are far from such edges. When creating a pattern using error-diffusion it is therefore mandatory to check for periodic patterns close to straight edges, or to extract a smaller patch from a larger pattern. Fig. 1 illustrates this issue showing that the microdot pattern close to the left border of the full pattern is periodic, and that a smaller patch far from the left edge is a more appropriate choice.

The pattern resulting from error diffusion is quasi-random. Diffraction due to large-scale periodic features is therefore avoided. The resulting pattern of microdots is non-periodic and the best tool to simulate the full apodizer is with a finite method to solve Maxwell's equations, such as the finite-difference time-domain method (FDTD).[14] However, the size of the ring apodizer is too large to be considered for FDTD with reasonable

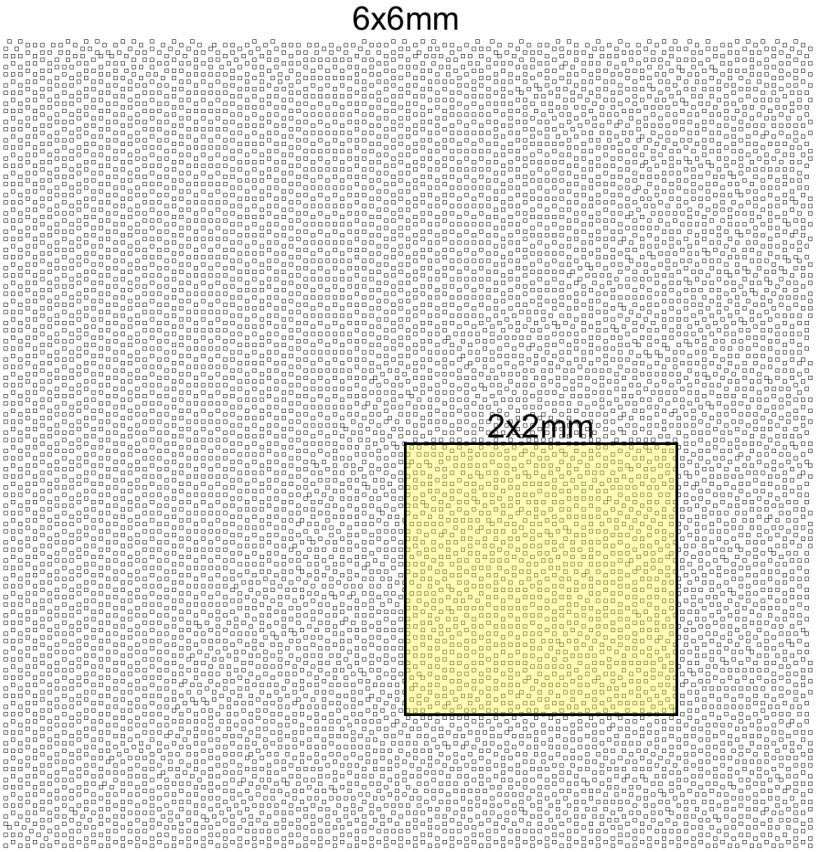

Figure 1. 6 mm × 6 mm microdot pattern showing periodic behavior close to the left edge due to a filling factor close to an integer fraction (25 % = 1/4). Clever selection of the 2 mm × 2 mm inset position is needed to obtain a semi-random pattern highlighted in yellow.

computational resources, and even a small patch is computationally expensive since the size of the dots is several times the wavelength. Therefore, RCWA simulations with a large unit cell are used to describe the field response of a quasi-periodic microdot pattern. Using large unit cells with 16 × 16 microdot pixels describes the local response of the microdots sufficiently well without introducing small scale periodic structures. The choice of 16 × 16 pixels in an RCWA simulation cell is a compromise between computational resources and accurate description of the semi-random pattern, resulting in approximately 100 CPU-hours of computation time per simulation. The accuracy of the results is also limited by the fraction of opaque pixels in the simulation cell since the filling factor is fixed to fractions of $16^2 = 256$. However, the results of these simulations show that the transmission and phase can be interpolated between these discrete filling factors to obtain the response of intermediate grayscale values. Fig. 2 shows an RCWA simulation result for a 16 × 16 pixels microdot pattern. The resulting quantities from the simulation are the phase step between the clear and the grayscale part of the apodizer and the transmission of the 0th order. For each microdot simulation a reference simulation of a clear section with no microdots is used to normalize the transmission and phase.

In principle, the transmission of a microdot pattern is defined by the filling factor of the pattern. The fraction of light falling on the chromium microdots is reflected, while the fraction falling between them is transmitted. However, since the microdot pattern is not operating in the subwavelength domain, non-zero orders are propagating. This means, that a significant part of the light is diffracted at low angles. In the coronagraph, only the 0th order is used, and higher orders have to propagate at sufficiently high angles to be intercepted by the pupil stops or straylight baffles and not affect the coronagraphic performance. When assessing

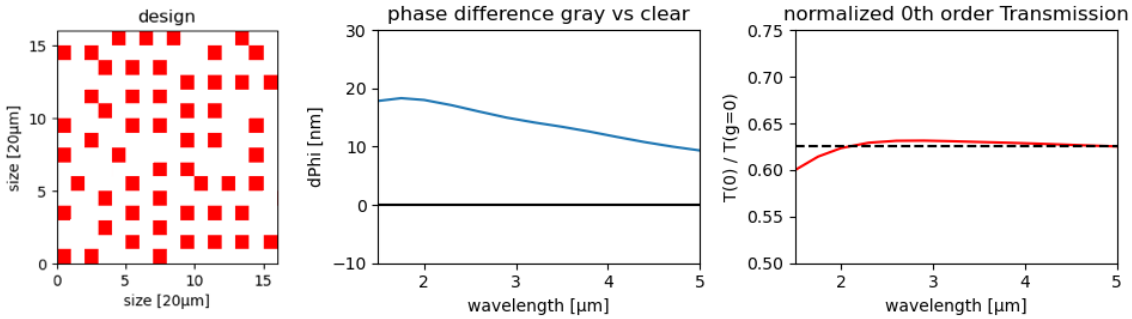

Figure 2. 16×16 microdot pattern design simulated with RCWA in the relevant wavelength range ($1.5-5\,\mu m$). Chromium microdots of $20\,\mu m$ width and $200\,nm$ thickness arranged in a pattern with 0.2148 filling factor were used here. Left: unit cell used in the RCWA simulations which is replicated periodically due to the periodic boundaries necessary for RCWA. Center: chromatic phase step between the microdot pattern and a clear region of the apodizer without microdots. Right: chromatic 0th-order intensity transmission normalized by the transmission of the clear region of the apodizer with no microdots. The nominal intensity transmission for the METIS ring apodizer of 62.5 % is shown as dashed line.

the microdot pattern, only the transmission in the 0th order is considered as metric which should match the 62.5 % intensity transmission needed for METIS. At the same time, light propagating in low diffraction orders has to be given careful consideration to avoid straylight or back-reflections from any component downstream of the ring apodizer. The RCWA simulations show that the typical amount of light diffracted in higher orders accounts for a total of around 10 % of the incoming light, and therefore could be a substantial source of straylight. Since the diffraction angles depend on the dot size, the microdots must be small enough to avoid light diffracted at small angles. For microdots of $< 20\,\mu m$ size, the lowest significant diffraction orders have intensities on the order of 10^{-5} and propagate at an angle of $0.5°$, which is high enough for the METIS straylight requirements.

To optimize the performance of the ring apodizer, the following parameters can be tuned: dot size, filling factor and chromium layer thickness. The dot size has an influence on the subwavelength behavior of the mask and has to be chosen large enough to avoid resonances due to subwavelength effects. At the same time, the pixel size influences the diffraction behavior of the ring apodizer, which requires the dots to be small enough to have the lowest significant diffraction orders at large enough angles from the optical axis. The range of filling factors has to be chosen to avoid integer fractions such as $25\,\% = 1/4$, resulting in periodic microdot patterns. Our simulations suggest that the optimal filling factor is close to this value for a nominal transmission of 62.5 % as required by METIS. The thickness of the chromium layer finally influences the optimal choice of filling factor, since a chromium layer $< 100\,nm$ transmits a certain amount of light in the considered wavelength range. A thin chromium layer also results in a larger differential optical path between K and L/M-band and a transmission which is more sensitive to small variations in the layer thickness. On the other hand, thick chromium layers are more complicated to manufacture.

A critical effect of the ring apodizer to be quantified is the phase step between the clear and the grayscale region. The METIS specifications require that the differential optical path between K and L/M-band should not be larger than $20\,nm$. This is due to the fact that the single conjugate adaptive optics (SCAO) system operates at K band, while the science bands used with the ring apodizer are the L and M-bands ($3-5\,\mu m$).

A series of simulations has been performed exploring the parameter space spanned by the dot size, filling factor and chromium layer thickness. The results are summarized in Fig. 3 showing the behavior of intensity transmission and phase step for the different parameters. Fig. 3 shows that the differential optical path increases with filling factor and decreases with increasing chromium layer thickness. This means that a thick chromium layer and small filling factor result in a lower differential optical path between K and L/M-bands. However, all parameters considered here are within the specifications of $20\,nm$.

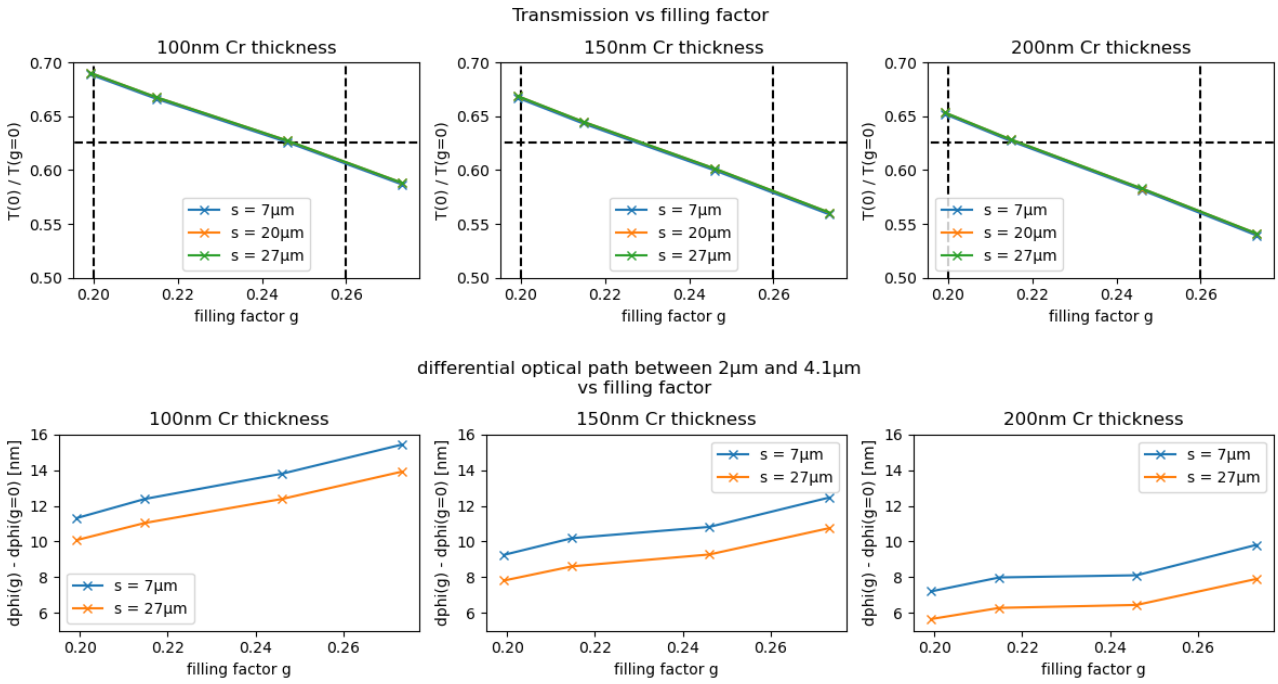

Figure 3. Intensity transmission (top) and differential optical path between K and L/M-band (bottom) for microdot patterns with different parameters. The intensity transmission is averaged in the range of $3-5\,\mu m$ corresponding to L and M-band, while the differential optical path is calculated between K ($2\,\mu m$) and L/M-band ($4.1\,\mu m$). Each subplot shows the results obtained for a certain chromium layer thickness. The differential optical path is always below the specification limit of 20 nm for METIS. For each chromium layer thickness, the nominal transmission of 62.5 % can be achieved by tuning the filling factor accordingly.

3. PROTOTYPE MANUFACTURING AND TESTING

Though the RCWA simulation framework describes the general behavior of the microdot patterns sufficiently well, it is not fully suited to describe the exact transmission and phase response of the aperiodic semi-random pattern. It is therefore mandatory to experimentally test the simulation results before manufacturing the ring apodizer. For this purpose, a set of test patterns with varying dot size and filling factor were manufactured on three prototype substrates (Ø 20 mm) with varying chromium layer thickness. The substrates are 2 mm thick ZnSe substrates coated with an antireflective coating and a protective SiO layer, procured from G&H Artemis Optical. The microdot patterns were made via chromium deposition by Opto-Line Inc. The parameters of the test samples are chosen to cover a certain range of the parameter space satisfying the requirements mentioned above and include a certain margin to compensate for imperfect simulation results and manufacturing tolerances. Each of the three prototypes has the same set of microdot test patterns imprinted on it. In this way, only one master pattern has to be produced, which is then transferred to the three substrates with different chromium layer thickness. The smallest chromium thickness is chosen to be 100 nm, which is the thickness at which chromium becomes sufficiently opaque across the considered wavelength range ($3-5\,\mu m$), and the highest value is chosen to be 200 nm, which is the limit of what can be provided by the manufacturer. Each of the substrates has the same design consisting of 25 test patterns arranged in a 5×5 grid featuring different combinations of dot size and filling factor. A schematic of the test pattern is shown in Fig. 4, including an inset showing the actual microdot pattern in one of the patterns and one of the three manufactured prototypes. The parameter space covered in this test design ranges from 7 to 27 µm dot size and from 0.20 to 0.26 filling factor. Each pattern is $2\,mm\times2\,mm$ with a 1 mm gap between patterns used as clear reference to measure the normalized transmission and phase step.

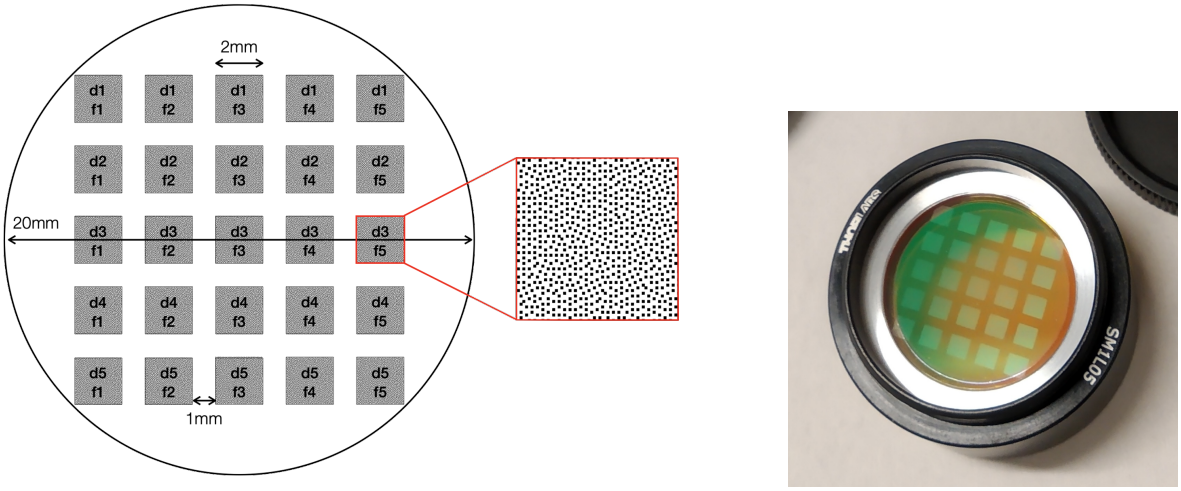

Figure 4. Microdot prototype patterns (left) and one of the three manufactured prototypes (right). The dot size ranges from 7 to 27 µm (d1-d5) and the filling factor ranges from 0.20 to 0.26 (f1-f5).

The three prototypes were tested on the VODCA coronagraphic testbench at ULiège[15] and allowed to define an optimal set of parameters providing the desired transmission and fulfilling the phase step requirement defined by METIS. The transmission of the prototypes was measured in pupil imaging mode on VODCA, and the median transmission of a 2 mm × 2 mm microdot pattern was normalized by the 1 mm clear region around it. The results agree with the RCWA simulations within a few percent. Note that it is possible to reach the target intensity transmission of 62.5 % with different combinations of dot size, filling factor and chromium thickness.

The phase step between the gray and clear parts of the pattern was measured using a Zernike wavefront sensor. A single Zernike mask optimized for 3.475 µm was used to measure the phase at both K and L/M-band. No significant signature of the microdot patterns was found within the measurement uncertainty, which is on the same order as the specification for the ring apodizer (20 nm rms). This agrees with our simulations, predicting a phase step of $0 - 20$ nm depending on the microdot parameters, and a phase step difference between K and L/M-band of $5 - 15$ nm.

The prototypes were further tested in a cryostat, where they were cooled down to 70 K repeatedly to confirm the robustness of the microdots and their adhesion to the substrate. The repeated cryogenic cycling was found to have no significant effect on the performance of the prototypes. The adhesion of the microdots to the substrate was further tested using an adhesive tape. The tape was gently pressed onto the microdot pattern and removed in order to assess the robustness of the microdot pattern. The tape test resulted in no significant damage of the microdots on the prototypes except for the thinnest chromium dots (100 nm). Therefore, a chromium thickness of 150 nm was chosen for the final METIS ring apodizer, providing a robust pattern and at the same time fulfill the specified transmission and phase step requirements.

4. METIS RING APODIZER

The ring apodizer would ideally be tailored to correct for the complex ELT pupil, including the non-circular edges and the presence of spider arms. However, the ring apodizer has to be placed in a pupil plane upstream the vortex phase mask, and the only available pupil plane is CFO-PP1, which is upstream the derotator. Therefore, the ring apodizer has to be circularly symmetric and can not correct, even partially, for spiders or other non-radial features of the ELT pupil. The edges of the clear and grayscale rings are slightly elliptical in order to account for the ellipticity of the pupil at CFO-PP1. In addition, the pattern includes an alignment mark to easily identify the orientation of the semi-major axis of the slightly elliptical pattern, and three uncoated clamping regions characteristic to the mount.

The final ring apodizer microdot pattern was created using the optimal parameters obtained from the testing of the three prototypes. The design and an image of the METIS ring apodizer are shown in Fig. 5. The final parameters are a filling factor of 0.23, dot size of 15 µm, and chromium thickness of 150 nm. The ring apodizer has been manufactured in June 2024 and will soon undergo further inspection and tests.

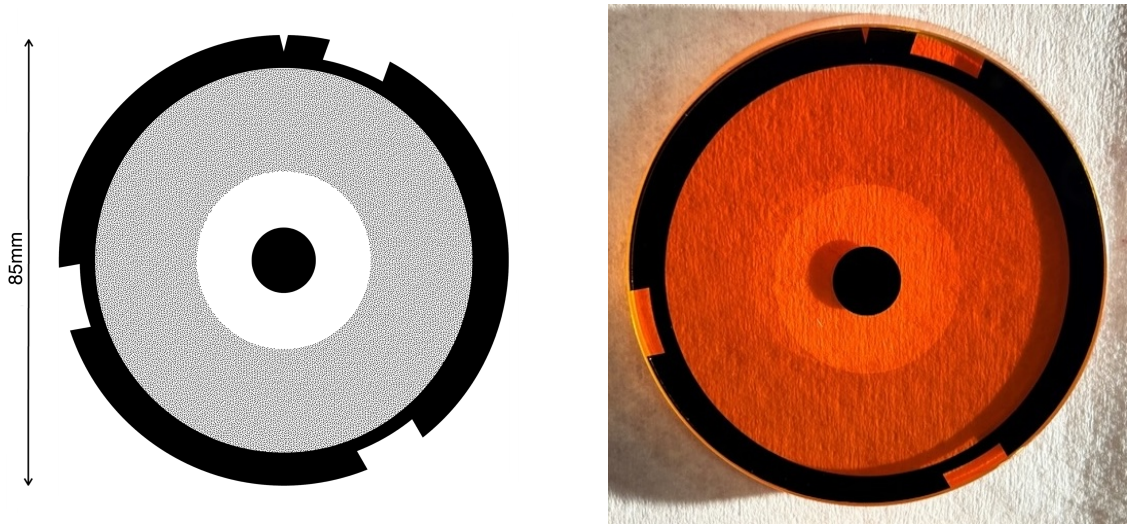

Figure 5. Design of the METIS ring apodizer (left) and final component (right). Note that the microdots in the left image are oversized by a factor of 10 for visibility.

5. CONCLUSION

The ring-apodized vortex coronagraph mode of the METIS instrument implements a vortex coronagraph adapted for the large central obscuration of the ELT. We have reported on the development of the METIS ring apodizer from design to manufacturing. We have simulated the underlying microdot technology for different parameters and optimized the pattern to match the requirements for METIS. We then manufactured three prototypes and tested them on our infrared coronagraphic testbench VODCA, as well as for the robustness of the microdot pattern. The transmission and phase response of the prototypes are in agreement with our simulations and the ring apodizer specifications. Based on the prototype characterization, we then produced the METIS ring apodizer design and manufactured the final component. Further testing of the ring apodizer will be concluded within the next weeks.

ACKNOWLEDGMENTS

This project has received funding from the European Research Council (ERC) under the European Union's Horizon 2020 research and innovation programme (grant agreement No 819155). Some of the required computational resources were provided by the Consortium des Équipements de Calcul Intensif (CÉCI), funded by the Fonds de la Recherche Scientifique de Belgique (F.R.S.-FNRS) under Grant No 2.5020.11, and by the Walloon Region.

REFERENCES

[1] Cirasuolo, M., Tamai, R., Koehler, B., Biancat-Marchet, F., Gonzáles Herrera, J. C., and ELT Team, "The Rise of the Giant: ESO's Extremely Large Telescope," *The Messenger* **192**, 3 (2024).

[2] Brandl, B., Bettonvil, F., van Boekel, R., Glauser, A., Quanz, S., Absil, O., Amorim, A., Feldt, M., Glasse, A., Güdel, M., Ho, P., Labadie, L., Meyer, M., Pantin, E., van Winckel, H., and METIS Consortium, "METIS: The Mid-infrared ELT Imager and Spectrograph," *The Messenger* **182**, 22–26 (2021).

[3] Absil, O., Kenworthy, M., Delacroix, C., Orban de Xivry, G., König, L., Pathak, P., Doelman, D., Por, E., Snik, F., Cantalloube, F., Carlotti, A., Courtney-Barrer, B., Dolkens, D., Glauser, A., van Boekel, R., Bertram, T., Feldt, M., Pantin, E., Quanz, S., Bettonvil, F., and Brandl, B., "Metis high-contrast imaging: from final design to manufacturing and testing," in [*Ground-based and Airborne Instrumentation for Astronomy X*], Society of Photo-Optical Instrumentation Engineers, SPIE (2024).

[4] Delacroix, C., König, L., Absil, O., Orban de Xivry, G., Forsberg, P., Karlsson, M., Ronayette, S., Pantin, E., and Barriere, J.-C., "The elt/metis annular groove phase masks," in [*Advances in Optical and Mechanical Technologies for Telescopes and Instrumentation VI*], Society of Photo-Optical Instrumentation Engineers, SPIE (2024).

[5] Mawet, D., Pueyo, L., Carlotti, A., Mennesson, B., Serabyn, E., and Wallace, J. K., "Ring-apodized Vortex Coronagraphs for Obscured Telescopes. I. Transmissive Ring Apodizers," *Astrophysical Journal Supplement Series* **209**(1), 7 (2013).

[6] Zhang, M., Ruane, G., Delorme, J.-R., Mawet, D., Jovanovic, N., Jewell, J., Shaklan, S., and Wallace, J. K., "Characterization of microdot apodizers for imaging exoplanets with next-generation space telescopes," in [*Space Telescopes and Instrumentation 2018: Optical, Infrared, and Millimeter Wave*], Lystrup, M., MacEwen, H. A., Fazio, G. G., Batalha, N., Siegler, N., and Tong, E. C., eds., **10698**, 106985X, International Society for Optics and Photonics, SPIE (2018).

[7] Martinez, P., Dorrer, C., Carpentier, E. A., Kasper, M., Boccaletti, A., Dohlen, K., and Yaitskova, N., "Design, analysis, and testing of a microdot apodizer for the apodized pupil lyot coronagraph," *Astronomy & Astrophysics* **495**(1), 363–370 (2009).

[8] Kasper, M. and Mawet, D., "Gearing up the sphere," *The Messenger* **149**(9), 17–21 (2012).

[9] Macintosh, B. A., Graham, J. R., Palmer, D. W., Doyon, R., Dunn, J., Gavel, D. T., Larkin, J., Oppenheimer, B., Saddlemyer, L., Sivaramakrishnan, A., Wallace, J. K., Bauman, B., Erickson, D. A., Marois, C., Poyneer, L. A., and Soummer, R., "The Gemini Planet Imager: from science to design to construction," in [*Adaptive Optics Systems*], Hubin, N., Max, C. E., and Wizinowich, P. L., eds., **7015**, 701518, International Society for Optics and Photonics, SPIE (2008).

[10] Trauger, J., Moody, D., Gordon, B., Krist, J., and Mawet, D., "A hybrid Lyot coronagraph for the direct imaging and spectroscopy of exoplanet systems: recent results and prospects," in [*Techniques and Instrumentation for Detection of Exoplanets V*], Shaklan, S., ed., **8151**, 81510G, International Society for Optics and Photonics, SPIE (2011).

[11] Moharam, M. and Gaylord, T., "Rigorous coupled-wave analysis of planar-grating diffraction," *Journal of the Optical Society of America* **71**(7), 811–818 (1981).

[12] Floyd, R. W. and Steinberg, L., "An Adaptive Algorithm for Spatial Greyscale," *Proceedings of the Society for Information Display* **17**(2), 75–77 (1976).

[13] Ulichney, R. A., "Dithering with blue noise," *Proceedings of the IEEE* **76**(1), 56–79 (1988).

[14] Taflove, A., Hagness, S. C., and Piket-May, M., "Computational electromagnetics: the finite-difference time-domain method," *The Electrical Engineering Handbook* **3**(629-670), 15 (2005).

[15] Jolivet, A., Orban de Xivry, G., Huby, E., Piron, P., Vargas Catalán, E., Habraken, S., Surdej, J., Karlsson, M., and Absil, O., "L- and m-band annular groove phase mask in lab performance assessment on the vortex optical demonstrator for coronagraphic applications," *Journal of Astronomical Telescopes, Instruments, and Systems* **5**(2), 025001 (2019).